JMEPEG (2019) 28:2672–2680
https://doi.org/10.1007/s11665-019-04053-8

1059-9495/$19.00

Microstructure and Mechanical Properties of Extruded Mg-7Sn-5Zn-*x*Al (*x* = 0, 1, 2 and 3 wt.%) Alloy

Jing Jiang, Tingqu Li, Guang-Li Bi, Feng-Yun Yan, Chi Cao, Yuan-Dong Li, and Ying Ma

(Submitted July 25, 2018; in revised form January 31, 2019; published online April 24, 2019)

Microstructure and mechanical properties of extruded Mg-7Sn-5Zn-*x*Al (*x* = 0, 1, 2 and 3 wt.%) alloy were investigated. The as-cast Mg-7Sn-5Zn alloy mainly comprised α-Mg dendrites, Mg_2Sn and nanosized Mg-Zn phases in a Mg matrix, whereas the quasicrystal (icosahedral (I)) phase precipitated with the addition of Al. After extrusion, the grain size decreased due to dynamic recrystallization and the resulting particles were crushed and distributed along the extrusion direction. The highest tensile strength was exhibited by the extruded Mg-7Sn-5Zn-2Al alloy, which had a yield strength, ultimate tensile strength and elongation to failure of 198, 343 MPa and 18.7%, respectively. The high tensile strength was mainly attributed to grain refinement and precipitation strengthening of the Mg_2Sn and icosahedral phases.

Keywords as-extruded Mg alloy, mechanical properties, Mg-Sn-Zn-Al alloy, microstructure

1. Introduction

As one of the lightest metallic materials, Mg alloys have attracted attention across a wide set of industries due to their low density, high specific strength and stiffness, good electromagnetic shielding characteristics and readiness to be recycled (Ref 1-4). Parts of Mg alloys have been applied to automobiles, 3C and the aerospace industry. However, the low tensile strength and poor ductility of Mg alloys at room temperature limit their development and application. Thus, it is necessary to explore new high-performance Mg alloys to further broaden their fields of application.

Recently, the relatively inexpensive Mg-Sn-based alloys have attracted considerable interest because of their moderate tensile strength and available elongation to failure, which are mainly due to precipitation strengthening of the Mg_2Sn phase (Ref 5-7). Great effort has been made to further improve the mechanical properties of Mg-Sn alloys, such as adding alloying elements (Ref 8-10), heat treatment (Ref 11, 12) and hot working (Ref 13, 14). Alloying is one of the most effective methods to enhance mechanical properties of Mg-Sn alloy by solution strengthening, grain refinement and precipitation strengthening (Ref 15-17). Zn and Al have been reported to be promising alloying elements for Mg-Sn alloys. The addition of Zn could precipitate multiple fine and homogeneous Mg-Zn particles due to its large solid solubility (~ 6 wt.%) in the Mg matrix at 340 °C (Ref 10, 18). Also, the precipitation of the Mg_2Sn phase could be promoted by incorporating Al. Wrought Mg-Sn-Zn-Al alloys display high tensile strength and superplasticity (Ref 19-23). Kim et al. (Ref 19) have reported that rolled Mg-7Sn-5Zn-2Al alloy sheets exhibit the highest yield strength (318 MPa) and ultimate tensile strength (373 MPa) as well as feature a reasonably large elongation to failure (8%). The high tensile strength of the alloys is mainly associated with the precipitation of the fine Mg_2Zn and icosahedral (I) phases in the α-Mg matrix. The investigation of Wang et al. (Ref 23) showed that the yield strength, ultimate tensile strength and elongation to failure of the extruded Mg-4Zn-1.5Al-2Sn alloy aged at 150 °C for 40 h are 236 MPa, 314 MPa and 18%, respectively. Sasaki et al. (Ref 12) have also pointed out that the yield strength and ultimate tensile strength of the extruded Mg-6.6Sn-5.9Zn-2.0Al-0.2Mn alloy under double aging (70 °C/150 h and 140 °C to the peak hardness) could reach 370 MPa and 399 MPa, respectively. Kim et al. (Ref 20) have demonstrated that the extruded Mg-8Sn-3Al-1Zn alloy exhibits a superplasticity (elongation of 450-1015%) at 250 °C with strain rates from 5×10^{-4} to 5×10^{-3} s^{-1} owing to the fine distribution of the Mg_2Sn phase.

As indicated, the high tensile strength of wrought Mg-Sn-based alloys is mainly related to the presence of Mg_2Sn during hot working or artificial aging treatment. Moreover, previous work has demonstrated that the addition of Al to the Mg-7Sn-5Zn alloy could form a new secondary solidification phase (icosahedral (I) phase) to enhance the tensile strength of the alloy (Ref 19). To further understand the effect of adding Al on the microstructure and mechanical properties of the Mg-7Sn-5Zn alloy, we prepared extruded Mg-7Sn-5Zn-*x*Al (*x* = 0, 1, 2 and 3 wt.%) alloy and systematically investigated the effects of different Al contents on the microstructure and mechanical properties of the extruded Mg-Sn-Zn alloy.

2. Experimental

Alloys with nominal compositions of Mg-7Sn-5Zn-*x*Al (*x* = 0, 1, 2 and 3 wt.%), which were designated as TZ75, TZA751, TZA752 and TZA753, respectively, were prepared from pure Mg, Sn and Zn in a graphite crucible under an anti-

Jing Jiang, Guang-Li Bi, Feng-Yun Yan, Chi Cao, Yuan-Dong Li, and **Ying Ma**, State Key Laboratory of Advanced Processing and Recycling of Nonferrous Metals, Lanzhou University of Technology, Lanzhou 730050, China; School of Material Science and Engineering, Lanzhou University of Technology, Lanzhou 730050, China; **Tingqu Li**, State Key Laboratory of Advanced Processing and Recycling of Nonferrous Metals, Lanzhou University of Technology, Lanzhou 730050, China; College of Materials Science and Engineering, Jilin Institute of Chemical Technology, Jilin 132022, China; and Hongbang Die Casting (Nantong) Co., Ltd., Nantong, China. Contact e-mail: glbi@163.com.

oxidizing flux. The melts were homogenized at 750 °C for 0.5 h and then poured into a water-cooling mold at 720 °C. The cylinder-shaped ingot with a diameter of 90 mm and height of 500 mm was homogenized at 480 °C for 12 h and then extruded into a bar. The cross section of extrusion die was a rectangle with a length of 50 mm and width of 7 mm, and the preheating temperature of extrusion die was 360 °C. The extrusion temperature, extrusion ratio and extrusion rate of ingot were 450 °C, 17:1 and 3 mm/s, respectively.

The microstructure, phase structure and composition of the extruded alloy were characterized by optical microscopy (OM, Olympus-GX71), x-ray diffraction (XRD; D8-ADVANCE), scanning electron microscopy (SEM, JSM-5600) with built-in energy-dispersive x-ray spectroscopy (EDS), high-resolution transmission electron microscopy (HRTEM) and selected area electron diffraction (SAED, JEM-2100F). The thin foil samples for the HRTEM observation were prepared using an ion polishing system (RES101). Specimens for OM and SEM were first ground on 400-, 600-, 800- and 1000-grit silicon carbide papers and etched after polishing in a solution of picric acid and 2% nitric acid for $\sim$ 5 s. The average grain size of extruded alloys was measured via a linear intercept method. Tensile tests were performed in an Instron 1211 tensile-testing machine at room temperature with a strain rate of 1×10^{-3} s^{-1} for all specimens. The tensile specimens (gauge length: 43 mm, width: 5 mm and thickness: 1.5 mm) were cut from the extruded bar along the extrusion direction. Tensile specimen and corresponding detailed schematic illustration are shown in Fig. 1(a) and (c). Three parallel tensile specimens of each extruded alloy were chosen for tensile testing, and the most stable tensile curve among three samples was considered the final tensile property of the extruded alloy. All specimens for microstructure observation and tensile testing were cut at the center of cross section composed of normal and transverse directions for extruded alloy bar (see Fig. 1b) in order to make sure the consistency and contrast of microstructure for the present alloys.

3. Results and Discussion

3.1 Microstructure

Figure 2 shows OM microstructures of the as-cast alloys. The as-cast TZ75 alloy mainly comprises α-Mg dendrites and a Mg_2Sn phase that mainly distributes throughout the inter-dendritic regions, as shown in Fig. 2(a) (Ref 22, 23). It is noted that some particles precipitate in the inter-dendritic regions (see Fig. 2b), and the volume fraction of particles slightly increases with the addition of Al. The XRD patterns of the as-cast alloys are presented in Fig. 3. Besides α-Mg and Mg_2Sn phases in the as-cast TZ75 alloy, diffraction peaks from the $Mg_{32}(Al,Zn)_{49}$ phase are observed in the as-cast TZA751, TZA752 and TZA753 alloys, whereas that of the Mg-Zn phase is not indexed in the XRD patterns for all alloys as the Mg-Zn phase only exists in trace amounts. The intensity of the Mg_2Sn phase diffraction peak increases with increasing Al content, which shows that the volume fraction of the phase increases with the addition of Al. The microstructure of the extruded alloy is shown in Fig. 4. After extrusion, α-Mg grains of the alloy are significantly refined from coarse dendrites to fine equiaxed grains with an average grain size of 22.8 μm due to the occurrence of dynamic recrystallization (Ref 21, 24). The grain size of the extruded alloys significantly decreases and reaches a minimum value when the Al content is 2% (see Fig. 4b, c, and d). The average grain sizes of the extruded TZA751, TZA752 and TZA753 alloys are approximately 16, 12 and 13 μm, respectively. Moreover, the particles in the as-cast alloys are crushed and distributed along the extrusion direction (see Fig. 4a). The SEM images of the extruded alloys in Fig. 5

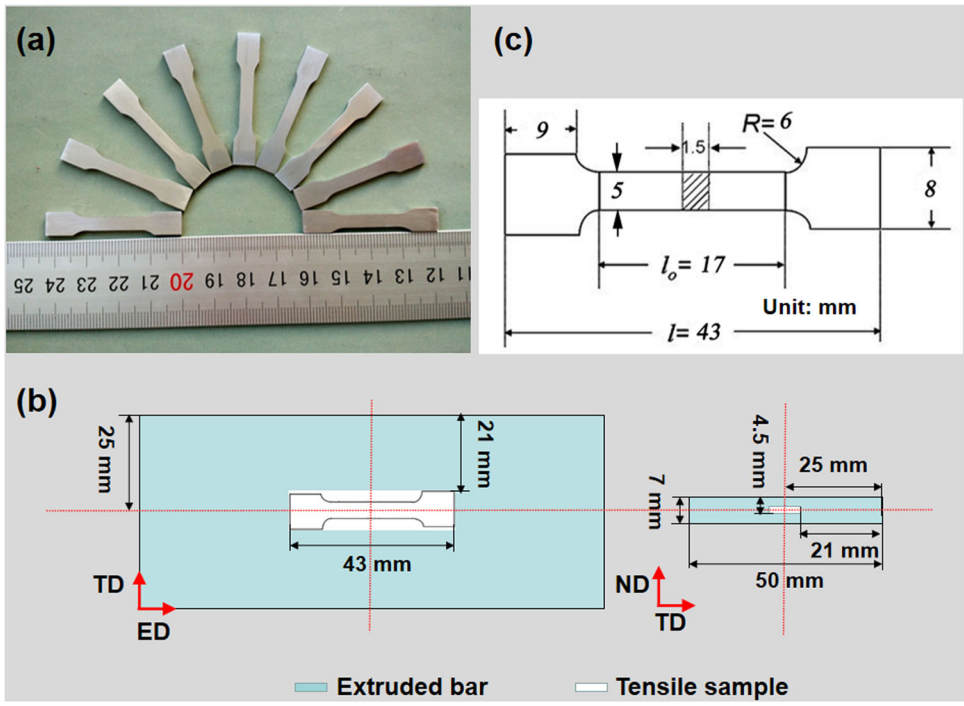

Fig. 1 Tensile sample (a) cut from extruded bar (b) and corresponding sketch map (c) of tensile sample

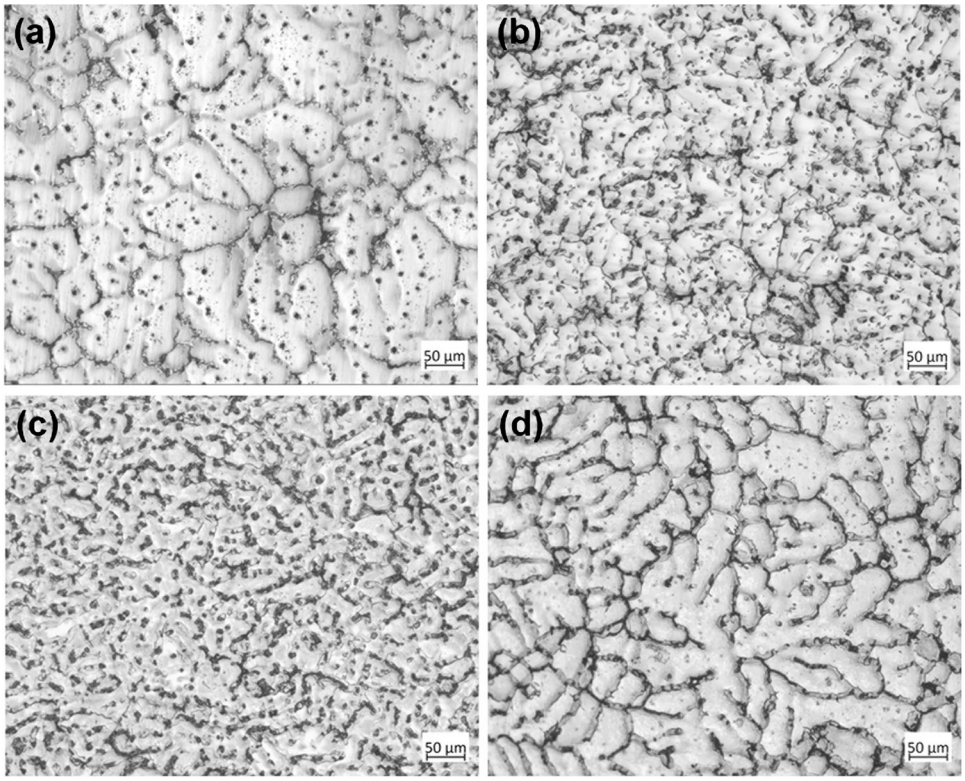

Fig. 2 Optical microstructures of as-cast alloys: (a) TZ75, (b) TZA751, (c) TZA752 and (d) TZA753

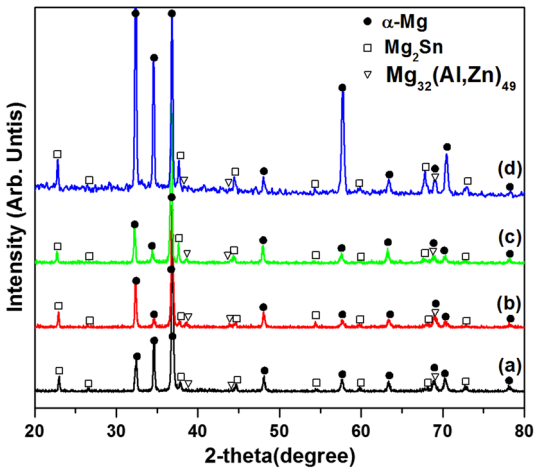

Fig. 3 XRD patterns of as-cast alloys: (a) TZ75, (b) TZA751, (c) TZA752 and (d) TZA753

indicate that the particles disperse more homogeneously with the addition of Al. The volume fraction of the particles increases with increasing Al content, as shown in Fig. 5(b), (c), and (d). This SEM observation is consistent with the XRD results in Fig. 3. According to the EDS results and corresponding literature (Ref 6, 22), the large irregular particle is Mg_2Sn as shown in Fig. 5. To further understand the structure of the fine particles in the Mg matrix, the particles in the extruded TZA753 alloy were examined by HRTEM and SAED, the image and pattern of which are shown in Fig. 6. It can be seen from Fig. 6(a) that three types of particles appear in the Mg matrix of the extruded TZA753 alloy; these are elliptical particles (marked as A), spherical particles (marked as B) and nanosized particles that are found in a high volume fraction. The SAED pattern of particle A indicates that the particle is Mg_2Sn (Fm3m; a = 0.522 nm) and is oriented with respect to Mg as follows (Ref 23): $(0\text{-}111)_{Mg}//(220)_{Mg2Sn}$ and $[1\text{-}213]_{Mg}//[21\text{-}1]_{Mg2Sn}$. According to the EDS data from particle B in Fig. 6(d), the chemical composition of the particle is Mg(62.1%)-Zn(21.5%)-Al(15.9%), which is similar to that of the I phase ($Mg_{47.2}Zn_{36.9}Al_{15.9}$) in the Mg-7Sn-5Zn alloy reported by Kim et al. (Ref 19). Considering the XRD results shown in Fig. 3, it can be concluded that particle B is I phase. The average size of the broken Mg_2Sn and I phases is determined to be 0.42 and 0.5 nm, respectively. Figure 6(b) shows the HRTEM image of typical nanosized particles that appear in two morphologies: one morphology is plate-shaped (marked as C; diameter: 2.5 nm; length: 8 nm), and the other morphology is rod-shaped (marked as D; diameter: 3 nm; length: 23 nm). Thus, the average particle size is approximately 9.1 nm, as determined by analyzing 10 HRTEM images. The SAED patterns in Fig. 6(e) and (f) indicate that the plate- and rod-shaped particles are Mg_2Zn and Mg_4Zn_7, which are β_1' and β_2' in Mg-Zn-based alloys, respectively (Ref 12, 25).

3.2 Mechanical Properties

The typical engineering stress–strain curves of the extruded alloys at room temperature are shown in Fig. 7. The corresponding mechanical properties of the extruded alloys are also listed in Table 1. The tensile strength and ductility of the extruded TZ75 alloy increase remarkably with increasing Al content. As the Al content is 1%, the extruded TZA751 exhibits the highest elongation to failure (ε) of 24%. When the addition

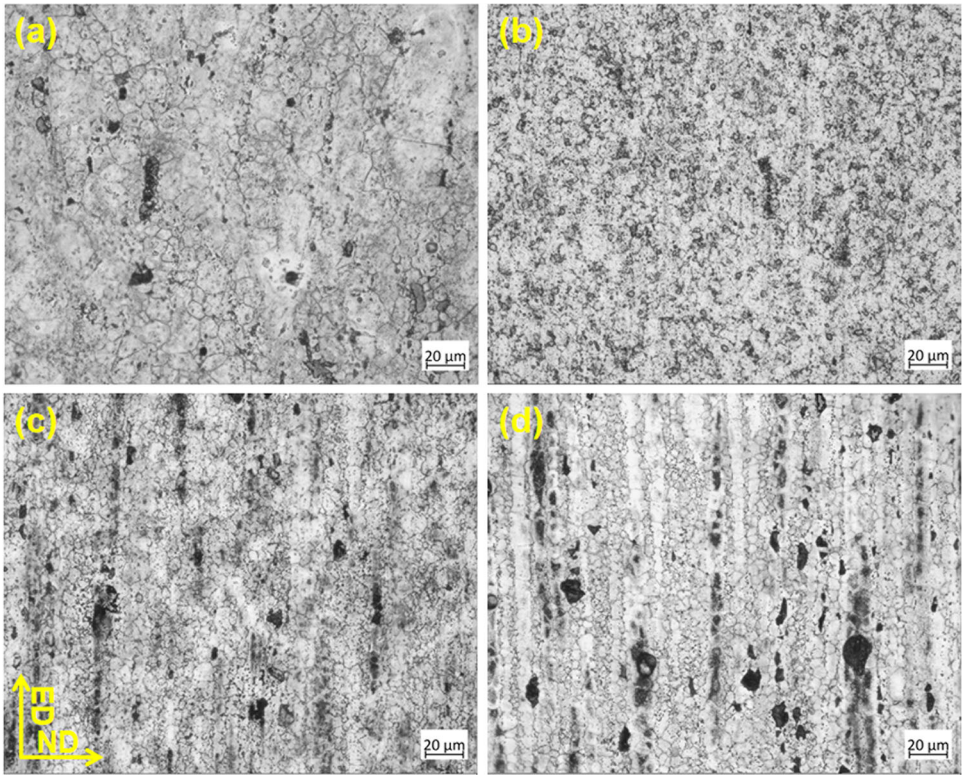

Fig. 4 Optical microstructures of extruded alloys: (a) TZ75, (b) TZA751, (c) TZA752 and (d) TZA753

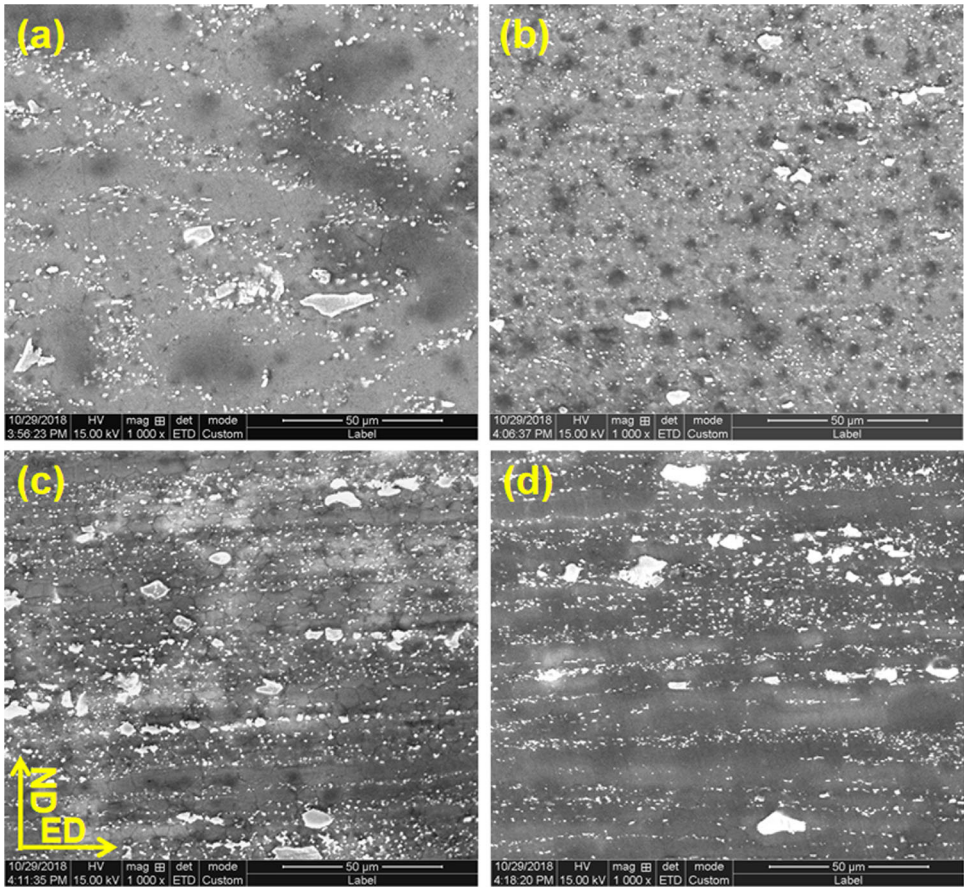

Fig. 5 SEM images of extruded alloys: (a) TZ75, (b) TZA751, (c) TZA752 and (d) TZA753

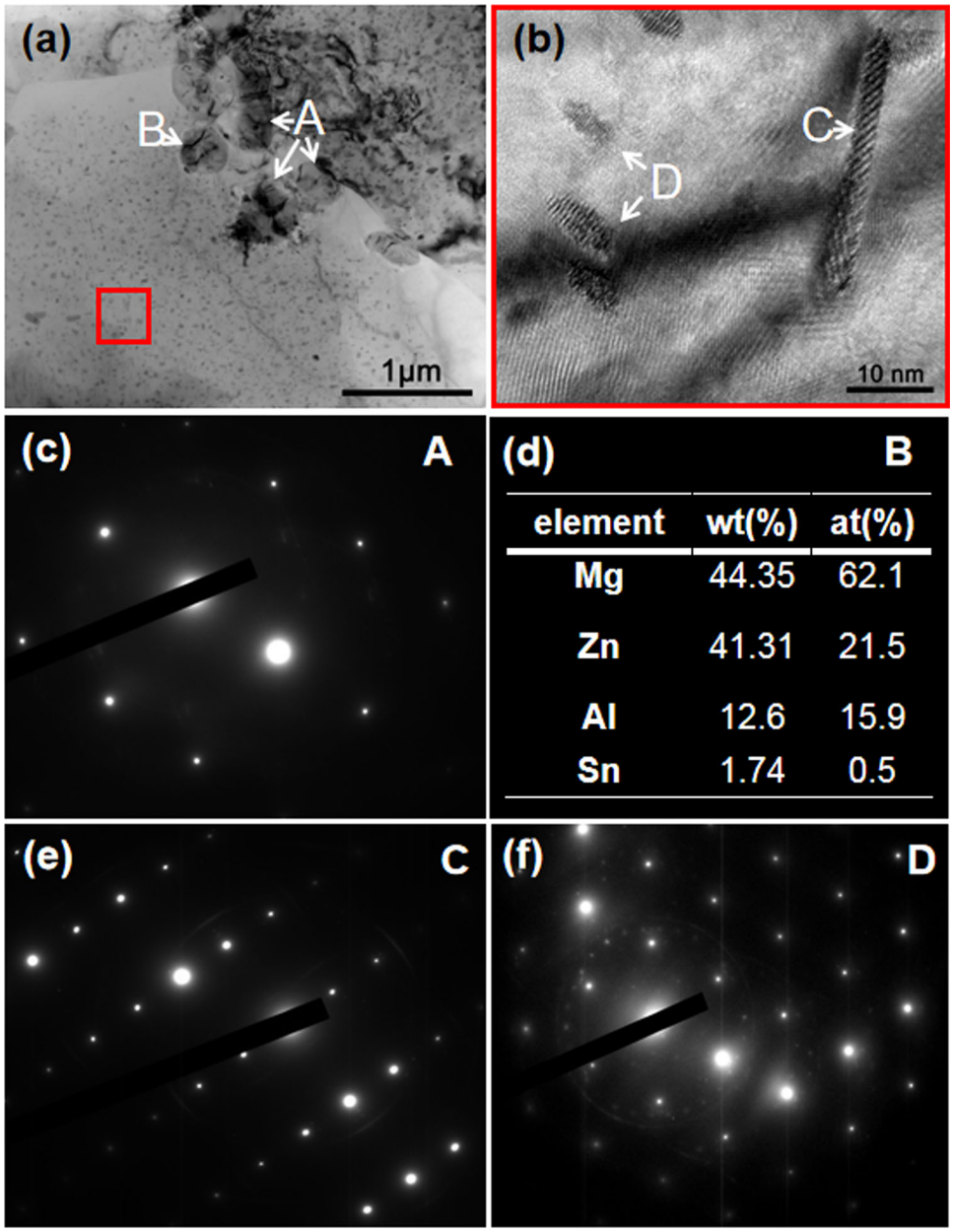

Fig. 6 TEM image (a), high-resolution TEM image (b) of particles in the red region in image (a) and corresponding SAED patterns of Mg_2Sn (c) and Mg-Zn particles (e) and (f) for extruded TZA753 alloy

of Al is 2%, the extruded TZA752 alloy exhibits the highest tensile strength, the yield strength ($\sigma_{0.2}$), ultimate tensile strength (σ_b) and ε are 198, 343 MPa and 18.7%, respectively. In comparison with the tensile strength of the extruded TZ75 alloy, the values of $\sigma_{0.2}$ and σ_b of the extruded TZ752 alloy increase by 13 and 15%, respectively. This result indicates that a small amount of Al ($< 2\%$) addition significantly improves the tensile strength and ductility of the extruded TZ75 alloy. However, excessive Al leads to a decrease of $\sigma_{0.2}$, σ_b and ε. When the content of Al is 3%, $\sigma_{0.2}$, σ_b and ε of the extruded TZ753 alloy are 186, 315 MPa and 21%. From these results, we can deduce that the optimal amount of Al addition to the TZ75 alloy is 2%.

It can be concluded from the microstructure analysis that the improved mechanical properties of the extruded TZ75 alloy are mainly attributed to grain refinement and particle strengthening. To distinguish the contribution of different strengthening effects to the tensile yield strength of the as-extruded alloys, the quantitative improvement of tensile strength is evaluated. First, grain boundary acted as a barrier and could effectively hinder dislocation movements and extend into the adjacent grains due to different misorientations (Ref 26). The grain boundary strengthening mechanism is usually described by the Hall–Petch relation (Ref 27) $\sigma_y = \sigma_0 + k_y d^{-1/2}$, where σ_y is the yield strength of the alloy, σ_0 is the friction stress, d is the grain size and k_y is the slope of the Hall–Petch curve. In the present investigation, the addition of Al refines the grain size of the alloys and all alloys have same casting and extruded process; thus, the yield strength increment of the alloy can be expressed as follows:

$$\Delta\sigma_{GR} = k_y\left(d^{-1/2} - d_0^{-1/2}\right), \quad \text{(Eq 1)}$$

where d and d represent the grain size of the extruded TZ75 alloy with and without Al, respectively. In pure Mg, the value of k_y is 220 MPa $\mu m_{1/2}$ (Ref 28, 29). As shown in Fig. 4, the extruded TZA752 alloy shows a grain size (12 μm) finer than those of the extruded TZ75 (22.8 μm), TZA751 (16 μm) and TZA753 (13 μm) alloys. As a result, the yield strength improvements originating from grain boundary strengthening are 8.8, 17.6 and 15.4 MPa for the extruded TZA751, TZA752 and TZA753 alloys, respectively, in comparison with the extruded TZ75 alloy. Therefore, it can be concluded that the refined grains improve the yield strengths of extruded alloys by hindering the dislocation movement. Meanwhile, the cross-slip could be activated due to the blocked dislocation, which could enhance the ductility of the alloy (Ref 30). So, the extruded TZ752 alloy exhibits high yield strength and ductility. Further, particle strengthening derived from the intersection between particles and dislocations usually occurs by the dislocation shearing soft particles or bypassing hard particles and then the dislocation loops appear around the particles. Generally, dislocation looping, which is also known as the Orowan model, describes the intersection of a dislocation with hard particles since only considerably small and relativity soft particles can be sheared by dislocations. The particle strengthening improvement related to the Orowan model is given as follows (Ref 31, 32):

$$\Delta\sigma_{\text{Orowan}} = \frac{0.13G_m b}{\lambda}\ln\frac{d_p}{2b}, \quad \text{(Eq 2)}$$

where G_m is the shear modulus (G = 16.6 GPa), b is the Burgers vector [b = 0.32 nm; (Ref 33)] and λ is the interparticle spacing, which can be calculated using Eq 3 (Ref 34):

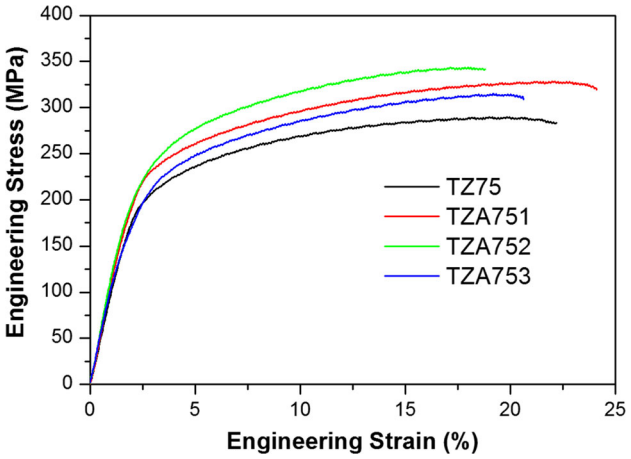

Fig. 7 Typical engineering stress–strain curves of extruded alloys at room temperature

$$\lambda \approx d_p\left[\left(\frac{1}{2V_p}\right)^{\frac{1}{3}} - 1\right] \quad \text{(Eq 3)}$$

where V_p is the volume fraction of particles. It can be seen from Eq 2 that σ_{Orowan} required to force a dislocation to glide between particles is inversely proportional to λ and d_p, but it is proportional to V_p (Ref 35). The values of λ, d_p and V_p of the particles of the present alloys are listed in Table 2. Due to their similar morphology and particle size, the Mg_2Sn and I phases are difficult to distinguish in SEM images; thus, measuring individual d_p values of these phases is not possible and the presented V_p value reflects their combination. The average d_p value of the combined Mg_2Sn and I phases is considered to be 0.46 μm. In addition, by measuring fewer than 10 HRTEM images for every extruded alloy, we found that the values of V_p and d_p of fine Mg_2Zn particles change very little with the addition of Al. Therefore, the yield strength arising from a Mg_2Zn particle strengthening effect is negligible. According to the values of λ in Table 2, the increase in the yield strength caused by particle strengthening is calculated to be 58.2, 129.7 and 94.6 MPa for the extruded TZA751, TZA752 and TZA753 alloys, respectively. Therefore, the role of grain refinement and particle strengthening in the extruded TZA752 alloy is more pronounced than that of the extruded TZA751 and TZA753 alloys. In contrast, the extruded TZA751 alloy has the lower volume fraction of particles (31.6%) and smaller grain size (16 μm) as compared with other three alloys. The dislocation slip is not fully restricted by these particles, and the microcracks are not easily formed because of the weak stress concentration (Ref 36). This can be confirmed by the tiny microcracks and uniform dimples in the later surface observation and fractograph (see Fig. 10). So, the extruded TZA751 alloy possesses the highest elongation to failure, while the extruded TZA752 alloy exhibits the maximum tensile strength.

3.3 Surface Observation and Fractograph

To further reveal the differences in the mechanical properties and fracture modes of the extruded alloys, the typical surface observation and fractographs of four extruded alloys are shown in Fig. 8, 9, 10 and 11. It can be found from Fig. 8(a), 9(a), 10(a) and 11(a) that the extruded alloys slightly undergo the necking phenomenon. In comparison with the other extruded alloys, the fracture direction of the extruded TZA752 alloy is nearly 90° with respect to the tensile direction, indicating that the alloy is fractured under positive shear stress. The high-resolution SEM images of the surface of the tensile specimens in Fig. 8(b), 9(b), 10(b) and 11(b) indicate that microcracks and macrocracks and slip traces appear on the surface of extruded alloys, respectively. It is noted that the direction of crack propagation is perpendicular to the tensile

Table 1 Mechanical properties of extruded alloys at room temperature

As-extruded alloys	Yield strength ($\sigma_{0.2}$, MPa)	Ultimate tensile strength (σ_b, MPa)	Elongation to failure (δ, %)
TZ75	172	289	22
TZA751	195	328	24
TZA752	198	343	18.7
TZA753	186	315	21

Table 2 Role of strengthening for extruded TZ75 alloy with different Al contents and corresponding microstructure analysis: the average grain size (d), yield strength increment of grain refinement ($\Delta\sigma_{GR}$), volume fraction of Mg_2Sn and I phase (V_{Mg_2Sn+I}), average particle size of Mg_2Sn and I phase (d_{Mg_2Sn+I}), average interparticle spacing of Mg_2Sn and I phase (λ_{Mg_2Sn+I}) and yield strength increment of particle strengthening ($\Delta\sigma_{Orowan}$)

Alloys	d, μm	$\Delta\sigma_{GR}$, MPa	V_{Mg_2Sn+I}, %	d_{Mg_2Sn+I}, μm	λ_{Mg_2Sn+I}, nm	$\Delta\sigma_{Orowan}$, MPa
TZA751	16	8.8	31.2	0.46	78	58.2
TZA752	12	17.6	40	0.46	35	129.7
TAZ753	13	15.4	37.1	0.46	48	94.6

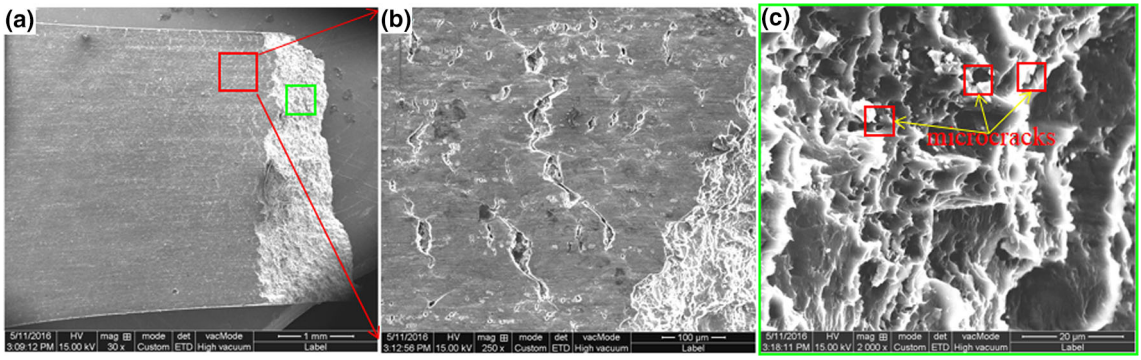

Fig. 8 Surface observation (a, b) and fractograph (c) of extruded TZ75 alloy at room temperature

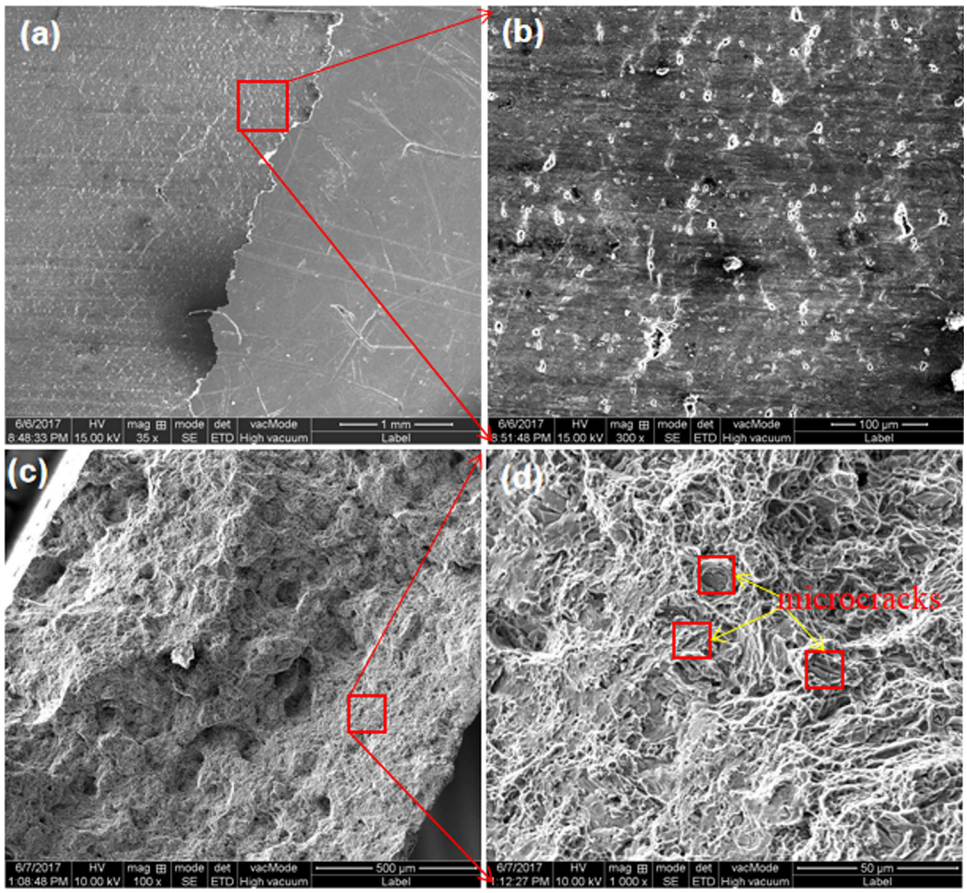

Fig. 9 Surface observation (a, b) and fractograph (c) of extruded TZA751 alloy at room temperature

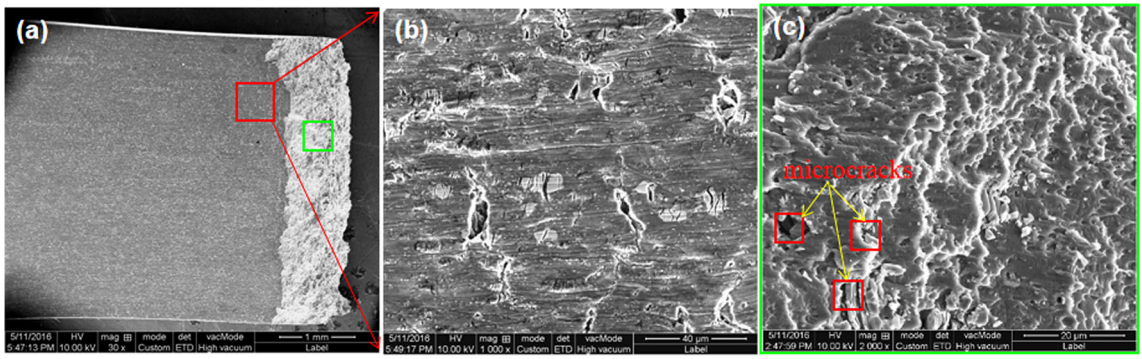

Fig. 10 Surface observation (a, b) and fractographs (c) of extruded TZA752 alloy at room temperature

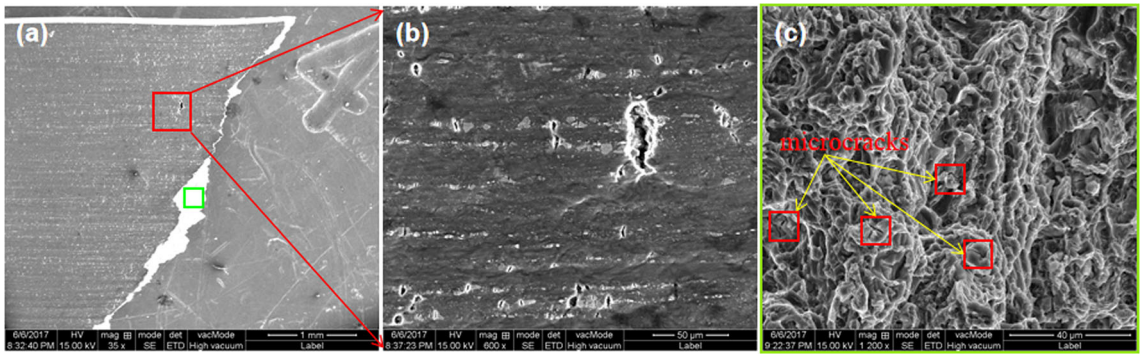

Fig. 11 Surface observation (a, b) and fractographs (c) of extruded TZA753 alloy at room temperature

direction, which also demonstrates that positive stress results in the nucleation and propagation of a crack. Additionally, fine microcracks and macrocracks observed around particles in the extruded TZA752 alloy are more than those found around the particles in the other extruded alloys. Generally, microcracks mainly initiate at the grain boundary or phase boundary, where stress concentration easily occurs due to dislocation pileup (Ref 36). Here, most crushed Mg_2Sn particles distributed at the grain boundaries and acted as effective crack sources, thereby releasing the stress concentration caused by inhibiting dislocation movement. The typical microcracks appearing around the particles were observed in the fractures of the extruded alloys (Fig. 8c, 9c, 10c, and 11c). Moreover, the fracture surface of the extruded TZ75, TZA752 and TZA753 alloys is flat and most cleavage planes with a few tearing ridges are seen on fracture surface, indicating that the fracture mode of the alloys is quasi-cleavage fracture. In contrast, the fracture surface of the extruded TZ751 alloy is rough with multiple tearing ridges and a lot of uniform dimples. This also demonstrates that the elongation to failure of the extruded TZ751 alloy is higher than that of the other three extruded alloys, which is consistent with mechanical properties in Fig. 7 and Table 1.

4. Conclusions

The microstructure and mechanical properties of extruded Mg-7Sn-5Zn-xAl (x = 0, 1, 2 and 3 wt.%) alloy have been investigated. Our conclusions are summarized as follows:

1. Besides α-Mg dendrites, Mg_2Sn and nanosized Mg-Zn phase in the Mg matrix, the $Mg_{32}(Al,Zn)_{49}$ phase with a quasicrystal structure precipitates in the as-cast Mg-7Sn-5Al alloy with the addition of Al. After extrusion, the grain size of the extruded alloy significantly decreases due to the occurrence of dynamic recrystallization; the second phases are crushed and distributed along the direction of extrusion.
2. The tensile strength of the extruded alloys initially increases and then decreases with the incorporation of Al content. When the Al content is 2%, the extruded Mg-7Sn-5Zn-2Al alloy exhibits the highest tensile strength and elongation to failure. The yield strength, ultimate tensile strength and elongation to failure of the alloy are 198, 343 MPa and 18.7%, respectively. The high tensile strength is mainly attributed to grain refinement and precipitation strengthening of the Mg_2Sn and icosahedral phases.

Acknowledgments

This work was financially supported by the National Nature Science Foundation of China (Nos. 51301082 and 51464031), Gansu Province Natural Science Foundations of China (Project Title: Microstructure and deformation behavior of extruded Mg-Dy-Zn(Cu,Ni) alloy with LPSO phase and 18JR3RA138) and Undergraduate Innovation and Entrepreneurship Training Programs (DC2018017 and DC2018022).

References

1. T.J. Chen, D.H. Zhang, W. Wang, Y. Ma, and Y. Hao, Effects of Nd or Zr Addition on Microstructure and Mechanical Properties of As-Cast Mg-Zn-Y Alloy, *Mater. Trans.*, 2016, **57**, p 1287–1295
2. T.J. Chen, D.H. Zhang, W. Wang, Y. Ma, and Y. Hao, Effects of Zn Content on Microstructures and Mechanical Properties of Mg-Zn-RE-Sn-Zr-Ca Alloys, *Mater. Sci. Eng. A*, 2014, **607**, p 17–27
3. Y. Zhang, X. Huang, Z. Ma, Y. Li, F. Guo, J. Yang, Y. Ma, and Y. Hao, The Influences of Al Content on the Microstructure and Mechanical Properties of As-Cast Mg-6Zn Magnesium Alloys, *Mater. Sci. Eng. A*, 2017, **686**, p 93–101
4. G. Li, J. Zhang, R. Wu, Y. Feng, S. Liu, X. Wang, Y. Jiao, Q. Yang, and J. Meng, Development of High Mechanical Properties and Moderate Thermal Conductivity Cast Mg Alloy with Multiple RE Via Heat Treatment, *J. Mater. Sci. Technol.*, 2018, **34**, p 1076–1084
5. H. Liu, Y. Chen, H. Zhao, S. Wei, and W. Gao, Effects of Strontium on Microstructure and Mechanical Properties of As-Cast Mg-5wt.% Sn alloy, *J. Alloys. Compd.*, 2010, **504**, p 345–350
6. J. Jiang, G. Bi, J. Liu, C.C. Ye, J. Lian, and Z. Jiang, Microstructures and Mechanical Properties of Extruded Mg-2Sn-*x*Yb (x = 0, 0.1, 0.5 at.%) Sheets, *J. Magn. Alloy.*, 2014, **2**, p 257–264
7. X. Yang, S. Wu, S. Lü, L. Hao, and X. Fang, Refinement of LPSO Structure in Mg-Ni-Y Alloys by Ultrasonic Treatment, *Ultraso. Sonochem.*, 2018, **40**, p 472–479
8. S.H. Huang, Microstructure and Mechanical Properties of a Ag Micro-Alloyed Mg-5Sn Alloy, *J. Mater. Eng. Perform.*, 2018, **27**, p 3199–3205
9. S. Zhu, T. Luo, T. Zhang, Y. Li, and Y. Yang, Effects of Cu Addition on the Microstructure and Mechanical Properties of As-Cast and Heat Treated Mg-6Zn-4Al Magnesium Alloy, *Mater. Sci. Eng. A*, 2017, **689**, p 203–211
10. N.E. Mahallawy, A.A. Diaa, M. Akdesir, and H. Palkowski, Effect of Zn Addition on the Microstructure and Mechanical Properties of Cast, Rolled and Extruded Mg-6Sn-xZn Alloys, *Mater. Sci. Eng. A*, 2016, **680**, p 47–53
11. J. Jiang, G. Bi, L. Zhao, R. Li, J. Lian, and Z. Jiang, Dry Sliding Wear Behavior of Extruded Mg-Sn-Yb Alloy, *J. Rare Earth.*, 2015, **33**, p 77–85
12. T.T. Sasaki, F.R. Elsayed, T. Nakata, T. Ohkubo, S. Kamado, and K. Hono, Strong and Ductile Heat-Treatable Mg-Sn-Zn-Al Wrought Alloys, *Acta Mater.*, 2015, **99**, p 176–186
13. S.H. Kim and S.H. Park, Influence of Ce Addition and Homogenization Temperature on Microstructural Evolution and Mechanical Properties of Extruded Mg-Sn-Al-Zn Alloy, *Mater. Sci. Eng. A*, 2016, **676**, p 232–240
14. G. Zhang, J. Chen, H. Yan, and B. Su, Effects of Solution Heat Treatment on Microstructure and Mechanical Properties of the Mg-4.5Zn-4.5Sn-2Al-0.6Sr Alloy, *J. Mater. Eng. Perform.*, 2014, **23**, p 3831–3841
15. L.L. Chang, H. Tang, and J. Guo, Strengthening Effect of Nano and Micro-sized Precipitates in the Hot-Extruded Mg-5Sn-3Zn Alloys with Ca Addition, *J. Alloys. Compd.*, 2017, **703**, p 552–559
16. H.D. Zhao, G.W. Qin, Y.P. Ren, W.L. Pei, D. Chen, and Y. Guo, Microstructure and Tensile Properties of As-Extruded Mg-Sn-Y Alloys, *Trans. Nonferrous Met. Soc. China*, 2010, **20**, p s493–s497
17. C.Y. Zhao, F.S. Pan, and H.C. Pan, Microstructure, Mechanical and Bio-corrosion Properties of As-Extruded Mg-Sn-Ca Alloys, *Trans. Nonferrous Met. Soc. China*, 2016, **26**, p 1574–1582
18. C. Liu, H. Chen, C. He, Y. Zhang, and J.F. Nie, Effects of Zn Additions on the Microstructure and Hardness of Mg-9Al-6Sn Alloy, *Mater. Charact.*, 2016, **113**, p 214–221
19. Y.K. Kim, S.W. Sohn, D.H. Kim, W.T. Kim, and D.H. Kim, Role of Icosahedral Phase in Enhancing the Strength of Mg-Sn-Zn-Al Alloy, *J. Alloys. Compd.*, 2013, **549**, p 46–50
20. B. Kim, J.G. Lee, and S.S. Park, Superplasticity and Load Relaxation Behavior of Extruded Mg-8Sn-3Al-1Zn Alloy at 250 °C, *Mater. Sci. Eng. A*, 2016, **656**, p 234–240
21. S.H. Park, H.S. Kim, and B.S. You, Improving the Tensile Strength of Mg-7Sn-1Al-1Zn Alloy Through Artificial Cooling During Extrusion, *Mater. Sci. Eng. A*, 2015, **625**, p 369–373
22. J. She, F. Pan, H. Hu, H. Pan, A. Tang, K. Song, Z. Yu, and S. Luo, Microstructures and Mechanical Properties of As-Extruded Mg-5Sn-1Zn-xAl (x = 1, 3 and 5) Alloys, *PNS MI*, 2015, **25**, p 267–275
23. B. Wang, F. Pan, X. Chen, W. Guo, and J. Mao, Microstructure and Mechanical Properties of As-Extruded and As-Aged Mg-Zn-Al-Sn Alloys, *Mater. Sci. Eng. A*, 2016, **656**, p 165–173
24. J. Yoon and S. Park, Forgeability Test of Extruded Mg-Sn-Al-Zn Alloys Under Warm Forming Conditions, *Mater. Des.*, 2014, **55**, p 300–308
25. K. Oh-Ishi, K. Hono, and K.S. Shin, Effect of Pre-aging and Al Addition on Age-Hardening and Microstructure in Mg-6 wt.% Zn Alloys, *Mater. Sci. Eng. A*, 2008, **496**, p 425–433
26. K. Ma, H. Wen, T. Hu, T.D. Topping, D. Isheim, D.N. Seidman, E.J. Lavernia, and J.M. Schoenung, Mechanical Behavior and Strengthening Mechanisms in Ultrafine Grain Precipitation-Strengthened Aluminum Alloy, *Acta Mater.*, 2014, **62**, p 141–155
27. C.S. Kim, I. Sohn, M. Nezafati, J.B. Ferguson, B.F. Schultz, Z. Bajestani-Gohari, P.K. Rohatgi, and K. Cho, Prediction Models for the Yield Strength of Particle-Reinforced Unimodal Pure Magnesium (Mg) Metal Matrix Nanocomposites (MMNCs), *J. Mater. Sci.*, 2013, **48**, p 4191–4204
28. B.Q. Shi, R.S. Chen, and W. Ke, Solid Solution Strengthening in Polycrystals of Mg-Sn Binary Alloys, *J. Alloys. Compd.*, 2011, **509**, p 3357–3362
29. C.H. Cáceres and A. Blake, The Strength of Concentrated Mg-Zn Solid Solutions, *Phys. Status Solidi A*, 2002, **194**, p 147–158
30. D.H. Bae, S.H. Kim, D.H. Kim, and W.T. Kim, Deformation Behavior of Mg-Zn-Y Alloys Reinforced by Icosahedral Quasicrystalline Particles, *Acta Mater.*, 2002, **50**, p 2343–2356
31. N. Tahreen, D.F. Zhang, F.S. Pan, X.Q. Jiang, D.Y. Li, and D.L. Chen, Strengthening Mechanisms in Magnesium Alloys Containing Ternary I, W and LPSO Phases, *J. Mater. Sci. Technol.*, 2018, **34**, p 1110–1118
32. Z. Zhang and D.L. Chen, Contribution of Orowan Strengthening Effect in Particulate-Reinforced Metal Matrix Nanocomposites, *Mater. Sci. Eng. A*, 2008, **483–484**, p 148–152
33. F. Naghdi, R. Mahmudi, J.Y. Kang, and H.S. Kim, Contributions of Different Strengthening Mechanisms to the Shear Strength of an Extruded Mg-4Zn-0.5Ca Alloy, *Philos. Mag.*, 2015, **95**, p 3452–3466
34. M.A. Meyers and K.K. Chawla, *Mechanical Behaviour of Materials*, Prentice Hall, Saddle River (NJ), 1999, p 492–494
35. J.G. Jung, S.H. Park, H. Yu, Y.M. Kim, Y.K. Lee, and B.S. You, Improved Mechanical Properties of Mg-7.6Al-0.4Zn Alloy Through Aging Prior to Extrusion, *Scr. Mater.*, 2014, **93**, p 8–11
36. J. Jiang, G. Bi, G. Wang, Q. Jiang, J. Lian, and Z. Jiang, Strain-Hardening and warm Deformation Behaviors of Extruded Mg-Sn-Yb Alloy Sheet, *J. Magn. Alloy.*, 2014, **2**, p 116–123